STAT3 couples activated tyrosine kinase signaling to the oncogenic core transcriptional regulatory circuitry of anaplastic large cell lymphoma

Nicole Prutsch[1], Shuning He[1], Alla Berezovskaya[1], Adam D. Durbin[1,2], Neekesh V. Dharia[1,3,9], Kelsey A. Maher[4], Jamie D. Matthews[5], Lucy Hare[5,6], Suzanne D. Turner[5,7], Kimberly Stegmaier[1,3], Lukas Kenner[8], Olaf Merkel[8], A. Thomas Look[1]*, Brian J. Abraham[4]* and Mark W. Zimmerman[1,10,11]*

[1] Department of Pediatric Oncology, Dana-Farber Cancer Institute and Boston Children's Hospital, Boston, MA, 02115

[2] Division of Molecular Oncology, St. Jude Children's Research Hospital, Memphis, TN, 38105

[3] Broad Institute of Harvard and MIT, Cambridge, MA 02141

[4] Department of Computational Biology, St. Jude Children's Research Hospital, Memphis, TN, 38105

[5] Division of Cellular and Molecular Pathology, Department of Pathology, University of Cambridge, Addenbrooke's Hospital, Cambridge, UK.

[6] Department of Pediatric Oncology and Hematology, Addenbrooke's Hospital, Cambridge, UK

[7] Faculty of Medicine, Masaryk University, Brno, Czech Republic

[8] Department of Pathology, Unit of Experimental and Laboratory Animal Pathology, Medical University of Vienna, Vienna, Austria

[9] Current affiliation: Genentech, South San Francisco, CA 94080

[10] Current affiliation: Foghorn Therapeutics, Cambridge, MA 02139

[11] Lead contact

*Email correspondence: brian.abraham@stjude.org, thomas_look@dfci.harvard.edu, mwz2002@gmail.com

Summary (150 words)

Anaplastic large cell lymphoma (ALCL) is an aggressive, CD30$^+$ T-cell lymphoma of children and adults. *ALK* fusion transcripts or mutations in the JAK-STAT pathway are observed in most ALCL tumors, but the mechanisms underlying tumorigenesis are not fully understood. Here we show that dysregulated STAT3 in ALCL co-occupies enhancers with master transcription factors, BATF3, IRF4, and IKZF1 to form a core regulatory circuit that establishes and maintains the malignant cell state in ALCL. Critical downstream targets of this network in ALCL cells include the proto-oncogene *MYC*, which requires active STAT3 to facilitate high levels of *MYC* transcription. The core auto-regulatory transcriptional circuitry activity is reinforced by MYC binding to the enhancer regions associated with *STAT3* and each of the core regulatory transcription factors. Thus, activation of STAT3 provides the crucial link between aberrant tyrosine kinase signaling and the core transcriptional machinery that drives tumorigenesis and creates therapeutic vulnerabilities in ALCL.

Introduction

Anaplastic large cell lymphoma (ALCL) is a CD30+ subtype of T-cell lymphoma, with around half of patients exhibiting chromosomal rearrangements involving the *ALK* gene[1–6]. Treatment with ALK inhibitors can achieve impressive complete responses in ALCL cells that express the *NPM1-ALK* fusion oncogene, and PDGFR inhibitors are effective for a subset of these patients[7]. However, long-term ALK inhibition can lead to relapse, and the overall survival for ALK-negative patients remains poor[8–11]. ALK-negative ALCLs have been found to harbor recurrent activating mutations in *JAK1*, *TYK2*, *ROS1,* and *STAT3*, each of which results in dysregulation of the JAK-STAT signaling pathway[12,13]. Recent preclinical studies of targeted therapy with tyrosine kinase inhibitors, such as JAK1/2 and TYK2 inhibitors, have shown efficacy in models of genetically defined ALK-negative ALCL subsets[7,13,14]. Otherwise, treatment strategies for ALK-negative patients are limited to chemotherapeutic regimens such as CHOP (cyclophosphamide, doxorubicin, vincristine, prednisone), which are usually ineffective at managing the disease[15].

The JAK-STAT pathway is a highly conserved signaling cascade activated by receptor tyrosine kinases in response to binding a wide range of cytokines and growth factors[16]. JAK-STAT and other signaling pathways provide most types of cells with a mechanism for relaying information from the extracellular microenvironment to the nucleus, where transcriptional effectors such as STAT3 regulate gene expression in a cell-type-specific manner[17]. However, the mechanisms explaining how STAT3 interacts

with cell-type-specific enhancers and how dysregulation of these pathways results in ALCL tumorigenesis are poorly understood.

In this study, we show activated of STAT3, a terminal effector of the JAK-STAT signaling pathway, interacts with a set of key transcription factors that form an interconnected autoregulatory loop termed the transcriptional core regulatory circuit (CRC) governing the ALCL gene expression program[18]. We show that this autoregulatory transcriptional loop consists of BATF3, IRF4, and IKZF1, and drives high levels of expression of each of these transcription factors due to positive feedback that each transcription factor exerts on the super- or stretch-enhancers (SE) associated with each of these genes[19,20]. As we and others have shown, STAT3 is activated downstream of ALK or due to direct mutation or fusion of genes including JAK1, JAK2, TYK2, or ROS1[12,13,21]. Aberrantly activated STAT3 binds concomitantly with each of the CRC transcription factors in small regions of ~1 kb of open chromatin within their super-enhancers as part of the autoregulatory loop of transcription factor genes, mediating high levels of expression of *MYC* and each member of the CRC. These results provide insights into the mechanisms by which oncogenic tyrosine kinase signaling pathways collaborate with CRC transcription factors to drive the oncogenic gene expression program in ALCL.

Results

Core regulatory transcription factors and STAT3 cooperate to drive the ALCL gene expression program

Based on prior work examining chromatin structure in pediatric leukemias and solid tumors, we began experiments to identify the transcriptional core regulatory circuit that mediates the oncogenic cell state in ALCL[22,23]. We first performed enhancer profiling using ChIP-seq for H3K27ac because genes encoding CRC transcription factors are generally regulated by large *cis*-regulatory elements called super- or stretch-enhancers. Super-enhancers are clusters of transcriptional enhancer elements that concentrate large amounts of the transcriptional machinery into biomolecular condensates capable of driving high levels of gene expression from target promoters[19,24]. A group of 38 genes encoding transcription factors were consistently associated with super-enhancers across at least five of eight analyzed ALCL cell lines, which include both ALK translocated and ALK-negative ALCL subtypes (Fig. 1a). ChIP-seq coverage tracks demonstrated that each of these genes is associated with a region very highly enriched with acetylation of H3K27, meeting the criteria for super-enhancer in all eight ALCL cell

lines, one ALCL patient-derived xenograft, and one primary patient ALCL (Fig. 1b-d). Next, we examined the expression levels of these three transcription factors in over 1200 cancer cell lines included in the Cancer Cell Line Encyclopedia[25]. We found that BATF3, IRF4, and IKZF1 are highly expressed in transcriptomic analyses from each of the ten ALCL cell lines included in this data set, as highlighted in red in Figure 1e-g. Thus, the very high level of expression of these three transcription factors in ALCL, regardless of whether individual cell lines have a translocated and activated *ALK* gene, led us to postulate that *BATF3*, *IRF4*, and *IKZF1* form an essential core regulatory circuit (CRC) that determines cell state in ALCL.

The CRC is an interconnected autoregulatory loop of super-enhancer-driven transcription factors that cooperatively regulate an extended network of genes that establishes cell state[18,26]. The enhancers associated with *BATF3*, *IRF4*, and *IKZF1* were each highly enriched in H3K27ac across all samples we examined, including NPM-ALK+ and ALK-negative cell lines (Fig. 2a). To test whether these transcription factors fulfill the interconnectivity requirements of CRC members, we performed CUT&RUN sequencing assays with antibodies specific for each of these factors to identify regions of sequence-specific genomic occupancy (Fig. 2b-d). For comparison, we also assayed the histone acetylation reader BRD4, and the MED1 component of the mediator complex. We found that BATF3, IRF4, and IKZF1 proteins each bind together within small regions of open chromatin (~1 kb) within their own and each other's regulatory enhancers. To demonstrate the interconnected regulation within this CRC, we used an antisense oligonucleotide (ASO) approach to mediate knockdown of the individual members of the CRC. Knockdown of each of the CRC members showed a pronounced and significant downregulation of BATF3, IRF4, and IKZF1 RNAs after 72 hours, thus affirming that each of these transcription factors is critical for the regulation of its own expression and those of each of the other two CRC transcription factors (see Supplemental Fig. S1). To demonstrate the effects of pharmacologic degradation of a single CRC component, we treated MAC2A ALCL cells with a series of IMiD compounds capable of degrading IKZF1 and found that IKZF1 disruption resulted in reduced cell growth and viability (Supplemental Figure S2a). In addition to being the most potent degrader of IKZF1, continuous treatment with these degraders for 5 days showed that Iberidomide was the most effective in reducing the growth of two different ALCL cell lines (Supplemental Fig. S2b and S2c). Thus, IKZF1, BATF3, and IRF4 form an interconnected, autoregulatory transcriptional loop, with single components being essential for ALCL cell growth, and IKZF1 being susceptible to targeted disruption.

STAT3 and the CRC transcription factors *BATF3*, *IRF4*, and *IKZF1* are selective gene dependencies in ALCL

Tumor-selective gene dependencies have been proposed as potential targets for cancer therapy because they are preferentially required for the growth and survival of tumor cells[27,28]. The DepMap Consortium has conducted genome-scale CRISPR-Cas9 dependency screens in over 1000 cancer cell lines, including five ALCL cell lines[28,29]. We analyzed these results and found a small group of genes that each qualifies as a selective dependency in ALCL cell lines compared to cancer cells derived from other lineages. Notably, the core regulatory transcription factors *BATF3*, *IRF4*, and *IKZF1* were selectively essential in ALCL cells compared to cell lines derived from other tumor types (Fig. 3a). ALCL cells were also selectively dependent on the signaling transcription factor *STAT3*, a terminal effector of the JAK-STAT pathway that has recently emerged as an attractive target in ALCL (Fig. 3a)[12,30]. Two additional non-transcription factor selective gene dependencies, *PTPN2* and *SBNO2*, were also revealed. *PTPN2* encodes a protein tyrosine phosphatase known to dephosphorylate JAK1 and STAT3[31–33]. PTPN2 has also been reported to regulate ALK phosphorylation and activity, with a potential role in resistance to ALK inhibition[34]. Less is known about *SBNO2*, a transcriptional co-regulator, which has been reported as a downstream target of IL-10 and STAT3 signaling in hematopoietic cells, both of which have also been shown to play a role in resistance to ALK inhibition in ALCL[35,36]. Overall, each of these selective gene dependencies in ALCL appears to be a member of the CRC or draws focus to the JAK-STAT signaling pathway as a crucial mediator of ALCL identity.

To test the contribution of STAT3, alone and in combination with Iberidomide, we treated three different cell lines with two different STAT3 inhibitors, STAT3-IN-3 or Stattic, and found that each of these inhibitors significantly reduced viable cell numbers after 72 hours (Supplemental Fig. S2d). Iberidomide also reduced the growth of these ALCL cells, as it did in the experiments shown in Supplemental Fig. S2b and c). The effects of these drugs in reducing cell growth were at least additive, as the combination of STAT3 inhibitors with Iberidomide yielded an even more remarkable and efficacious reduction in ALCL cell growth, as demonstrated in Supplemental Figure S2d.

ALCL tumors frequently harbor driver translocations activating the *ALK* tyrosine kinase receptor or mutations activating components of JAK-STAT signaling pathways[12]. The terminal signaling effector of either event is the activation of STAT3, which becomes hyper-phosphorylated, dimerizes, and then enters the nucleus to bind to its genomic signal response elements to activate key target genes in a sequence-dependent manner[21,37–39]. Based on this information and our finding of selective *STAT3*

dependency in ALCL, we focused on the role of STAT3 and its interaction with the CRC. We first examined the extent of localized H3K27ac by ChIP-seq, marking potential enhancers near the *STAT3* gene. The *cis*-regulatory enhancers associated with *STAT3* did not meet the quantitative H3K27ac enrichment threshold for a super-enhancer in most ALCL cells, despite high expression levels of both STAT3 transcript and protein in ALCL (Supplemental Fig. S3). Instead, high occupancy of BATF3, IRF4, IKZF1, and STAT3 was primarily detected at the *STAT3* promoter (Fig. 3b). We conclude that *STAT3* lacks a conserved autoregulatory super-enhancer in ALCL cells and therefore did not meet our algorithmic criteria for defining a CRC transcription factor gene.

However, consistent with collaboration between STAT3 and the CRC, genome-wide occupancy analysis showed that the STAT3 protein binds concomitantly with BATF3, IRF4, and IKZF1 at H3K27ac-marked regions throughout the genome (Fig. 3c). Unlike most transcription factors, STAT3 is highly dependent on post-transcriptional regulation through phosphorylation and dimerization downstream of activation of tyrosine kinases such as ALK or JAK family members[37]. Therefore, STAT3 functions as a signal-responsive transcription factor ordinarily dependent on the stimulation of receptor tyrosine kinases before it is activated to cooperate with CRC transcription factors in controlling gene expression[24]. This concept can also explain why the expression of *STAT3* is observed in many cell types, but dependency on STAT3 is restricted to ALCL and a limited number of other cell types where STAT3 signaling is active (Supplemental Fig. S3b). In ALCL cells, STAT3 occupancy was observed at super-enhancers associated with CRC transcription factors indicating a role in reinforcing the expression of this positive feedback loop (Fig. 3d). These results demonstrate that dysregulation of STAT3 by NPM-ALK or other driver mutations allows it to function as a *de facto* CRC component in ALCL, collaborating with BATF3, IRF4 and IKZF1 to establish an oncogenic transcription program and malignant cell state.

Activated STAT3 collaborates with CRC transcription factors to drive *MYC* expression

Upon activation, signaling transcription factors become highly concentrated at gene enhancers that are co-occupied by core regulatory transcription factors[24]. In order to understand the effects of activated STAT3 on the tumor transcriptome, we performed spike-in normalized mRNA-seq analysis on MAC2A (PCM1-JAK2+) cells treated with the JAK1/2 inhibitor ruxolitinib, and JB6 (NPM-ALK+) cells treated with the ALK inhibitor crizotinib, to determine fold-change in global transcript levels at 24 h (Fig. 4a,b). Notably, *MYC* transcript levels (highlighted in red; Fig 4a,b) were among the most significantly downregulated in both cell lines (Fig 4a, b, Supplemental Fig. S4). Next, we performed ChIP-

seq/CUT&RUN with an antibody specific for STAT3 in three ALCL cell lines – JB6 (ALK+), MAC2A (ALK-), FE-PD (ALK-), and an ALK+ PDX model – and found that STAT3 localizes with the CRC transcription factors BATF3, IRF4, IKZF1 at multiple epicenters across an super-enhancer region associated with the *MYC* gene suggesting that STAT3 cooperates with all three CRC transcription factors in the regulation of MYC expression (Fig. 4c,d, Supplemental fig. S5). As shown in Supplemental Figure S6, incubation of both JB6 and MAC2A cells for 72 hrs with the MYC-specific antisense oligonucleotide (ASO) mediated significantly reduced MYC RNA expression levels. ASO-mediated knockdown of MYC also significantly reduced mRNA expression levels of BATF3 and IKZF1 in both the MAC2A and JB6 cell lines, thus supporting coregulation of MYC and CRC members (Supplemental Fig. S6).

An immunoblotting time course of MAC2A cells treated with ruxolitinib, and JB6 cells treated with crizotinib, indicated a complete loss of phosphorylation of STAT3 (Y705) by 1 h following treatment initiation (Fig. 4e,f). Furthermore, after the loss of detectable STAT3 phosphorylation, MYC protein levels were significantly reduced, consistent with the essential role of activated STAT3 for high levels of expression of the *MYC* oncogene in ALCL (Fig. 4e,f).

STAT3 activation is necessary and sufficient for *MYC* expression and ALCL cell survival

To conclusively determine whether activation of STAT3 by NPM-ALK is the critical event required for high levels of *MYC* expression and cell viability in ALCL cells, we tested whether a mutationally activated, phosphomimetic STAT3 protein could rescue the effects of ALK inhibition in JB6 cells. These cells were transduced with a lentivirus encoding an mEGFP-tagged STAT3^{Y640F}-mutant cDNA. Mutation of the *STAT3* gene, such as the gain-of-function Y640F substitution, where the codon for tyrosine-640 is altered to encode for phenylalanine, is often observed as a somatic mutation in ALK-negative ALCL tumors[12]. First, we compared the LD_{50} values of JB6 control (parental) and STAT3^{Y640F}-expressing cells when challenged with ALK inhibitors. We found that the LD_{50} is 3-10 fold higher in STAT3^{Y640F} cells for both crizotinib and alectinib, indicating that activation of STAT3 is sufficient to rescue ALCL cell viability downstream of NPM-ALK inhibition (Fig. 5a), which has also been shown in the context of IL10RA[36]. Control and STAT3^{Y640F}-expressing JB6 cells were then treated with crizotinib and alectinib at 100 nM each, and cell growth was monitored daily for 72 hours. During treatment, control cells rapidly lost viability and failed to proliferate (Fig. 5b). By contrast, STAT3^{Y640F}-expressing cells continued proliferating, further demonstrating that direct activation of STAT3 can rescue cell growth and survival of ALK+ ALCL cells treated with an ALK tyrosine kinase inhibitor (Fig. 5b).

Next, we sought to assess the biochemical effects of the ALK kinase inhibitor crizotinib on STAT3 phosphorylation in control JB6 cells and cells expressing the STAT3^{Y640F} mutant protein by immunoblotting with a phospho-STAT3 (Y705) antibody (Fig. 5c). Six hours after treatment with 100 nM crizotinib, both the control and transduced JB6 cells exhibited loss of phosphorylation of the endogenous (unmutated) STAT3 protein. By contrast, the STAT3^{Y640F} mutant protein showed no reduction of phosphorylation at Y705 following treatment with crizotinib, indicating that it remains active despite inhibition of NPM-ALK (Fig. 5c). Since our results in Figure 4 indicated that STAT3 is an essential regulator of *MYC* gene transcription, we assayed *MYC* transcript levels by quantitative RT-PCR immediately following treatment with crizotinib in control and STAT3^{Y640F} cells. Three hours following the addition of 100 nM crizotinib, *MYC* mRNA levels were reduced by 50% in control cells compared to cells expressing STAT3^{Y640F}, which retained high levels of *MYC* RNA expression that were equivalent to the levels in untreated cells (Fig. 5d). These results demonstrate that rescuing STAT3 activity with a gain-of-function mutation, resulting in constitutive STAT3 phosphorylation independent of ALK, is sufficient to retain high levels of *MYC* expression and preservation of ALCL cell viability despite the inhibition of ALK with small molecule kinase inhibitors.

STAT3 and MYC invade enhancers driving CRC transcription factors

MYC family proteins have an essential role in promoting transcription initiation and elongation, and overexpression of MYC in tumor cells causes general amplification across the transcriptome of the cell[40,41]. Highly abundant MYC proteins in tumor cells have the potential to invade the super-enhancers of highly expressed genes by binding to lower affinity E-boxes, such that MYC increases the transcriptional output and reinforces oncogenic expression programs[42,43]. To assess the genomic co-occupancy of enhancers by MYC in ALCL, we performed CUT&RUN sequencing for MYC in MAC2A (*PCM1-JAK2*+) and JB6 (*NPM-ALK*+) cells. Along with BATF3 and STAT3, MYC binding was strongly enriched at super-enhancers, including those associated with the CRC transcription factor genes *BATF3*, *IRF4* and *IKZF1* (Fig. 6a-c, Supplemental Fig. S7a-c), as well as the typical enhancer and promoter driving *STAT3* and large super-enhancer region associated with *MYC* (Fig. 6d,e, Supplemental Fig. 7d,e). This indicates that MYC expression also participates in a positive feedback loop, which includes the *STAT3* enhancer and promoter, and functions as a component of the CRC by binding and occupying the super-enhancers that control the expression of their own genes and each of the other CRC transcription factors (Fig. 6f).

Discussion

Aberrant activation of signaling pathways downstream of tyrosine kinase proteins can drive abnormal cell growth and survival, leading to oncogenic transformation[38,44–47]. In ALCL, previous studies have converged on the JAK-STAT pathway as the central driver of ALCL tumorigenesis, with STAT3 as a critical terminal effector[12]. In NPM-ALK+ ALCL, STAT3 is activated by NPM-ALK, either directly or through intermediate JAK pathway kinases, and is required for cell survival and maintaining the neoplastic phenotype of ALCL cells[36,48]. The ALK-negative subtype of ALCL frequently harbors activating mutations in *JAK1*, *ROS1*, *TYK2* or *STAT3* directly, indicating a critical role for STAT3 activation in both subtypes[12]. Although STAT3 activation provides essential pro-growth signals required for ALCL tumorigenesis, it is not fully understood how exactly STAT3 facilitates the malignant identity of ALCL cells.

Chromatin profiling, enhancer mapping, and selective expression have recently emerged as useful strategies to identify oncogenic transcription factor networks that are necessary for the growth and survival of transformed tumor cells[49–52]. Our previous work in ALCL used enhancer profiling to reveal a signaling module through which the activated IL2R receptor cooperatively regulates transcription with the master transcription factor BATF3[53]. This finding highlighted the critical interplay between IL2R signaling and transcriptional regulation and indicated that treatments targeting these essential pathways could be successful at managing the disease. Here, we link BATF3, IKZF1, and IRF4 together in an autoregulatory transcriptional loop called the CRC. The IL2RA and IL2RB enhancers are bound by each of the CRC members, implying that these key receptors are part of the downstream regulatory targets of the ALCL CRC (Supplemental Fig. S8). Thus, rather than acting alone, BATF3 acts as part of a multicomponent system that regulates the ALCL malignant cell state. In addition, we link MYC transcription with the ALCL CRC and show that MYC expression requires the activation of STAT3 by tyrosine kinase signaling, which is highly active in both ALK+ and ALK- ALCLs.

Profiling the enhancer landscape of NPM-ALK+ and ALK-negative ALCL by H3K27ac ChIP-seq identified a conserved set of super-enhancers associated with highly expressed genes that encode transcription factors, several of which have been implicated in the pathogenesis of ALCL[27,54–56] (Fig. 1). Among these highly expressed transcription factor genes, we demonstrate that *BATF3*, *IRF4*, and *IKZF1*, are genetic dependencies in ALCL and act as part of a super-enhancer-regulated "cell identity intrinsic" interconnected autoregulatory loop (Fig. 2). Core regulatory transcription factors have

emerged as highly selective gene dependencies across a broad range of tumor types[18,22,23,57]. The gene regulatory activity of the CRC is essential for driving a lineage-specific transcription program and maintaining cell state[18].

ALCL cells were not only selectively dependent on this small group of core regulatory transcription factors, but they were also dependent on *STAT3* (Fig. 3). Unexpectedly, STAT3 does not meet our criteria for a CRC component since an autoregulatory super-enhancer does not drive its expression. Rather, it is activated as a "signal sensing" transcription factor whose expression is not always super-enhancer-regulated but can participate in affecting enhancers of CRC transcription factors when activated as an independent event through tyrosine phosphorylation. Once activated, STAT3 occupancy is restricted to enhancers already occupied by the CRC, which likely explains why activation of conserved signaling pathways can have disparate effects in different cell types that express unique combinations of CRC transcription factors. Thus, STAT3 belongs to a class of proteins referred to as "signaling transcription factors," which are activated by signaling cascades and then bind cooperatively to enhancers to exert conditional effects on the cellular transcriptome[58,59]. In this sense, signaling transcription factors provide an additional level of regulation, allowing cytokine signaling to regulate transcription via enhancers also occupied by the CRC transcription factors. The ability of cytokine binding to launch signaling pathways downstream of cell receptors, like tyrosine phosphorylation of STAT3, may function as an “on-off switch” for activation of the underlying CRC[24]. In the case of ALCL, the receptor signaling aspect usually required for STAT3 activation is subverted by the expression of constitutively active tyrosine kinases that have become disconnected from their normal conditional activation by cytokines produced by surrounding signaling cells. Furthermore, in ALCL the promiscuity of STAT3 in binding most active enhancers is unusual, as a smaller subset of enhancers is usually directly targeted by signaling transcription factors.

Additionally, we demonstrate that, once activated, STAT3 binds to the regulatory super-enhancers of *MYC*, driving high levels of *MYC* expression and permitting MYC to co-regulate the ALCL CRC (Fig. 4, 6). Other tumor types frequently employ direct amplification of the *MYC* gene[60,61], or enhancer hijacking from highly expressed genes by genomic structural rearrangements[62,63]. However, in ALCL tumor cells, activation of STAT3 provides a mechanism of *MYC* activation that is usually controlled by ligand-receptor signaling, but in this tumor is provided by constitutively activated ALK or JAK tyrosine kinases. Here we demonstrate the essential role of activated STAT3 in driving *MYC* expression by showing that the expression of a hyperactive $STAT3^{Y640F}$ mutant protein can rescue *MYC* levels, along with the loss of cell growth and viability observed following treatment with ALK inhibitors (Fig. 5). Unlike the normal

STAT3 protein that is dephosphorylated during ALK inhibitor treatment, the STAT3^{Y640F} mutant protein remains in the activated form with phosphorylation at Y705 even without ALK signaling. The essential role of phosphorylated (active) STAT3 in the transformation of ALCL, whether NPM-ALK+ or ALK-negative, suggests that treatments targeting STAT3 directly could be an effective treatment strategy for ALK-negative or ALK-inhibitor resistant ALCL[38,48].

Activated STAT3 and the CRC transcription factors each represent strong tumor-selective gene dependencies in ALCL, regardless of *ALK* status. As the relationship between oncogenic signaling pathways and transcriptional regulatory proteins becomes further resolved, targeted therapeutic strategies that exploit the interconnectedness of these dependencies will become attractive options for new therapies.

Limitations of the study

While conclusions of this study are supported by a broad range of samples, including cell lines and patient-derived cells, a comprehensive understanding of the core regulatory circuits and transcriptional networks driving human ALCL will likely require additional primary tumors with common and rare driver mutations and consider intra-tumor heterogeneity as well. Additionally, reduced CRC gene expression following MYC knockdown does not rule out the possibility that these transcription factors are downregulated indirectly, since reduction in MYC activity reduces the overall pool of biomolecular ingredients needed for transcription. The direct effect of MYC on CRC gene expression via binding to their associated enhancers, relative to the indirect contribution through binding promoters of its canonical target genes, is an unresolved question in the field.

Acknowledgments

This work was supported by NIH grants R35CA210064 (A.T.L.), R35CA210030 (K.S.) and K08CA245251 (A.D.D), and the St. Jude Children's Research Hospital Collaborative Research Consortium on 3D Regulatory Nuclear Landscape of Pediatric Cancer Cells (A.T.L., K.S., B.J.A.). N.P. was supported by a grant from the Lymphoma Research Foundation. A.D.D. and B.J.A. are supported by the American Lebanese Syrian Associated Charities (ALSAC). N.V.D. was supported by the Julia's Legacy of Hope St. Baldrick's Foundation Fellowship. SDT is supported by the project National Institute for Cancer Research (Programme EXCELES, ID Project No. LX22NPO5102) - Funded by the European Union - Next Generation EU and SDT, JDM and LH by the Cancer Research UK Cambridge

Centre [CTRQQR-2021\100012]. M.W.Z. was supported by grants from Alex's Lemonade Stand Foundation, Charles A. King Trust, and Claudia Adams Barr Foundation.

Author contributions

N.P., A.T.L., B.J.A. and M.W.Z. conceived and designed the study. N.P., S.H., A.B., and M.W.Z. performed experiments, N.P., S.H., A.B., K.A.M., J.D.M., L.H., S.D.T., L.K., O.M., A.D.D., N.V.D. and K.S performed data analysis and interpretation. N.V.D., K.A.M. and B.J.A. performed computational experiments and data analysis. A.T.L., B.J.A. and M.W.Z. jointly supervised the study. Writing, reviewing, and editing was performed by all authors.

Declaration of interests

K.S. is a member of the SAB and has stock options in Auron Therapeutics and received grant funding from Novartis and KronosBio on topics unrelated to this manuscript. B.J.A. is a shareholder in Syros Pharmaceuticals. N.V.D. is currently an employee of Genentech, Inc., and is a stockholder in Roche. A.T.L. is a shareholder in LightHorse Therapeutics and is a consultant/advisory board member for LightHorse Therapeutics and Omega Therapeutics. M.W.Z. is currently an employee and shareholder in Foghorn Therapeutics. The other authors declare no competing interests.

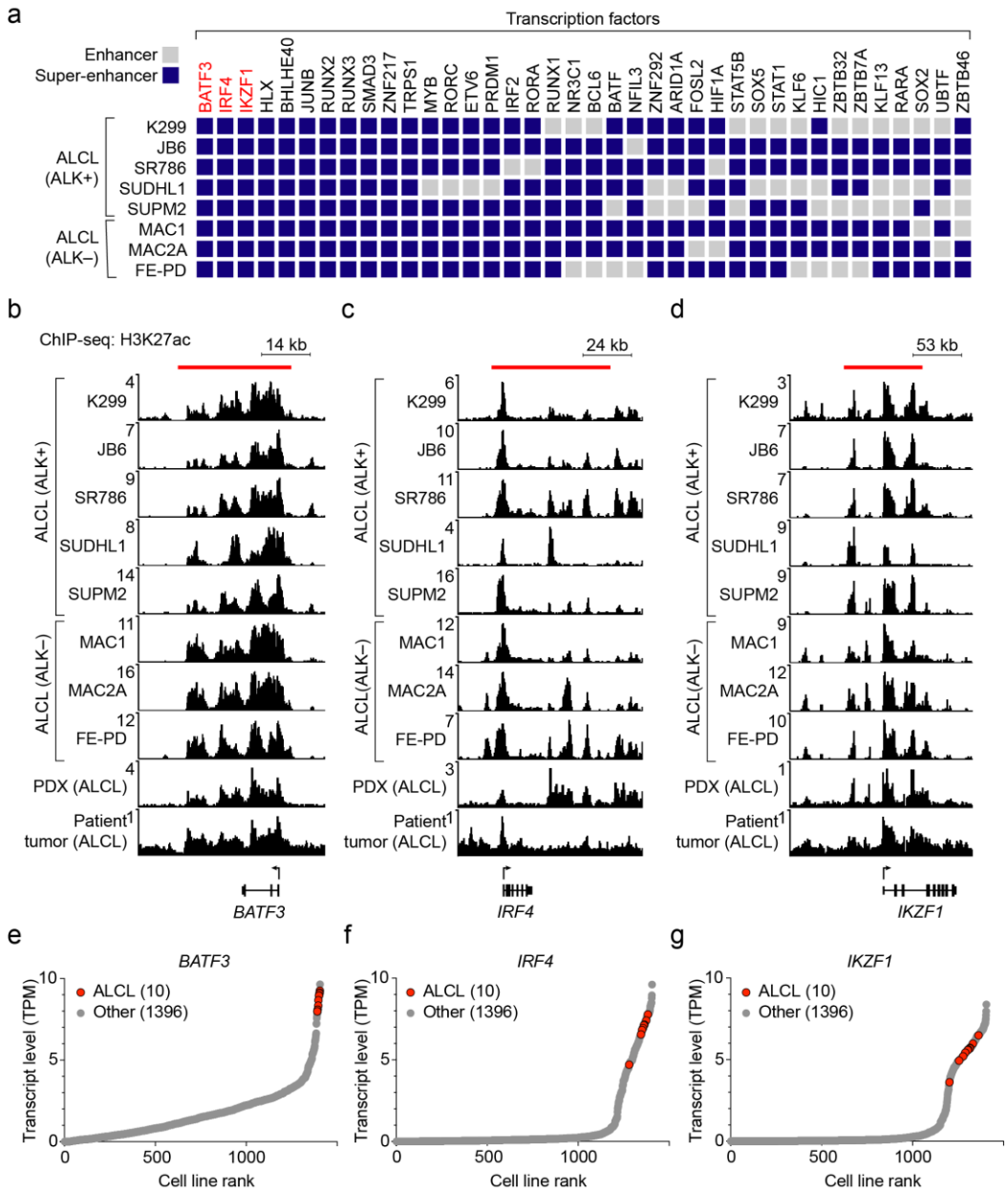

Figure 1. Highly selectively expressed transcription factors are associated with super-enhancers in human ALCL. a) Enhancer profiling of ALCL cell lines revealed a conserved set of super-enhancers associated with transcription factor encoding genes (n=38). Highlighted in red are super-enhancer-associated transcription factors that are also dependencies in ALCL (see Fig 3a). b-d) Normalized ChIP-seq alignment tracks for H3K27ac reveal enhancer regions associated with the *BATF3* (b), *IRF4* (c) and *IKZF1* (d) gene loci in ALCL. ChIP-seq read densities (y-axis) were normalized to reads per million reads sequenced from each sample. Red bars indicate the location of super-enhancers. e-g) Transcript levels (y-axis) of *BATF3* (e), *IRF4* (f) and *IKZF1* (g), ranked by gene expression (x-axis) across cell lines. Ten ALCL cell lines (shown in red) are compared to n=1396 cell types derived from other lineages (shown in gray).

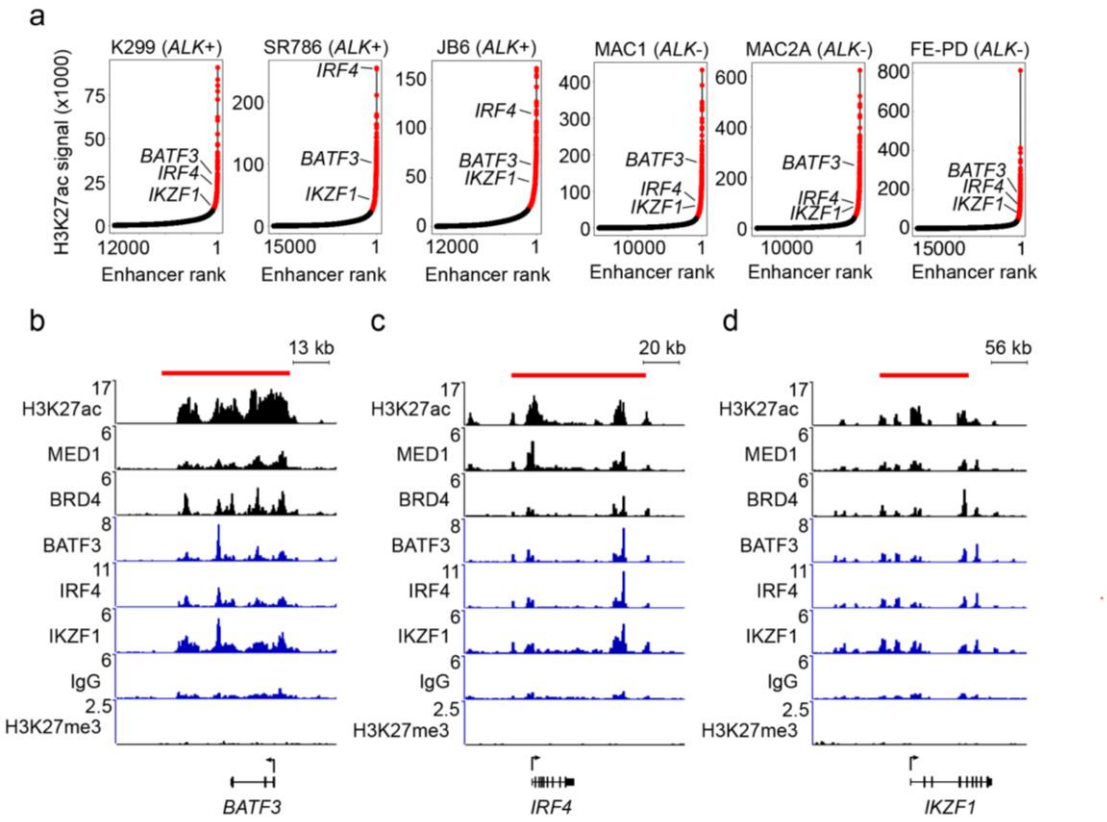

Figure 2. Identification and validation of an interconnected core transcriptional regulatory circuit in ALCL. a) Ranking of enhancers by H3K27ac signal associated with genes in *NPM-ALK*+ (K299, SR786, and JB6) and *ALK*– (MAC1, MAC2A, and FE-PD) ALCL cells. *BATF3*, *IRF4,* and *IKZF1* were associated with super-enhancers across all ALCL cell lines. b-d) CUT&RUN sequencing alignment tracks for MED1, BRD4, BATF3, IRF4, IKZF1 as well as IgG and H3K27me3 (controls) in MAC2A cells, overlaid with H3K27ac ChIP-seq, shown at the gene loci for *BATF3* (b), *IRF4* (c), and *IKZF1* (d). Read densities (y-axis) were normalized to reads per million reads sequenced in each sample.

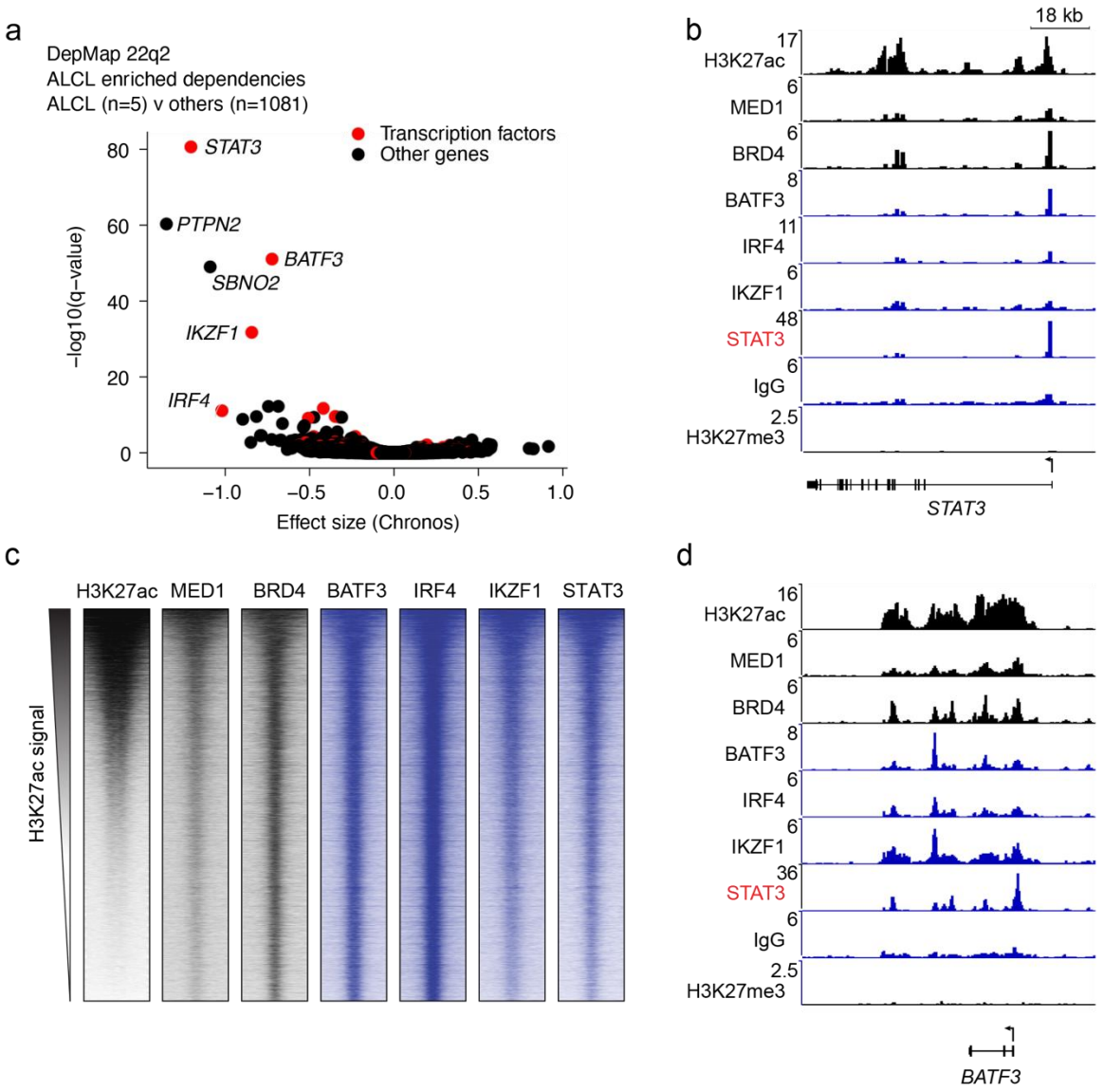

Figure 3. Tumor-selective gene dependencies in ALCL include the CRC and STAT3. a) Scatter plot showing dependency effect size (x-axis) and ALCL selectivity (y-axis) for all protein-coding genes. Genes encoding transcription factors are highlighted in red, and all other protein classes are shown in black. b) CUT&RUN sequencing alignment tracks for MED1, BRD4, BATF3, IRF4, IKZF1, STAT3 as well as IgG and H3K27me3 (controls) in MAC2A cells, overlaid with H3K27ac ChIP-seq at the *STAT3* locus. Gray bar indicates the location of a typical enhancer peak. c) Genome-wide co-occupancy for H3K27ac, MED1, BRD4, BATF3, IRF4, IKZF1, and STAT3 determined by ChIP-seq/CUT&RUN sequencing. Genomic regions (rows) were defined as those enriched in sequencing reads for at least one target and are ranked by the H3K27ac signal therein. d) CUT&RUN sequencing alignment tracks for MED1, BRD4, BATF3, IRF4, IKZF1, STAT3 and IgG (control) in MAC2A cells, overlaid with H3K27ac ChIP-seq at the *BATF3* locus. Red bar indicates the location of a super-enhancer.

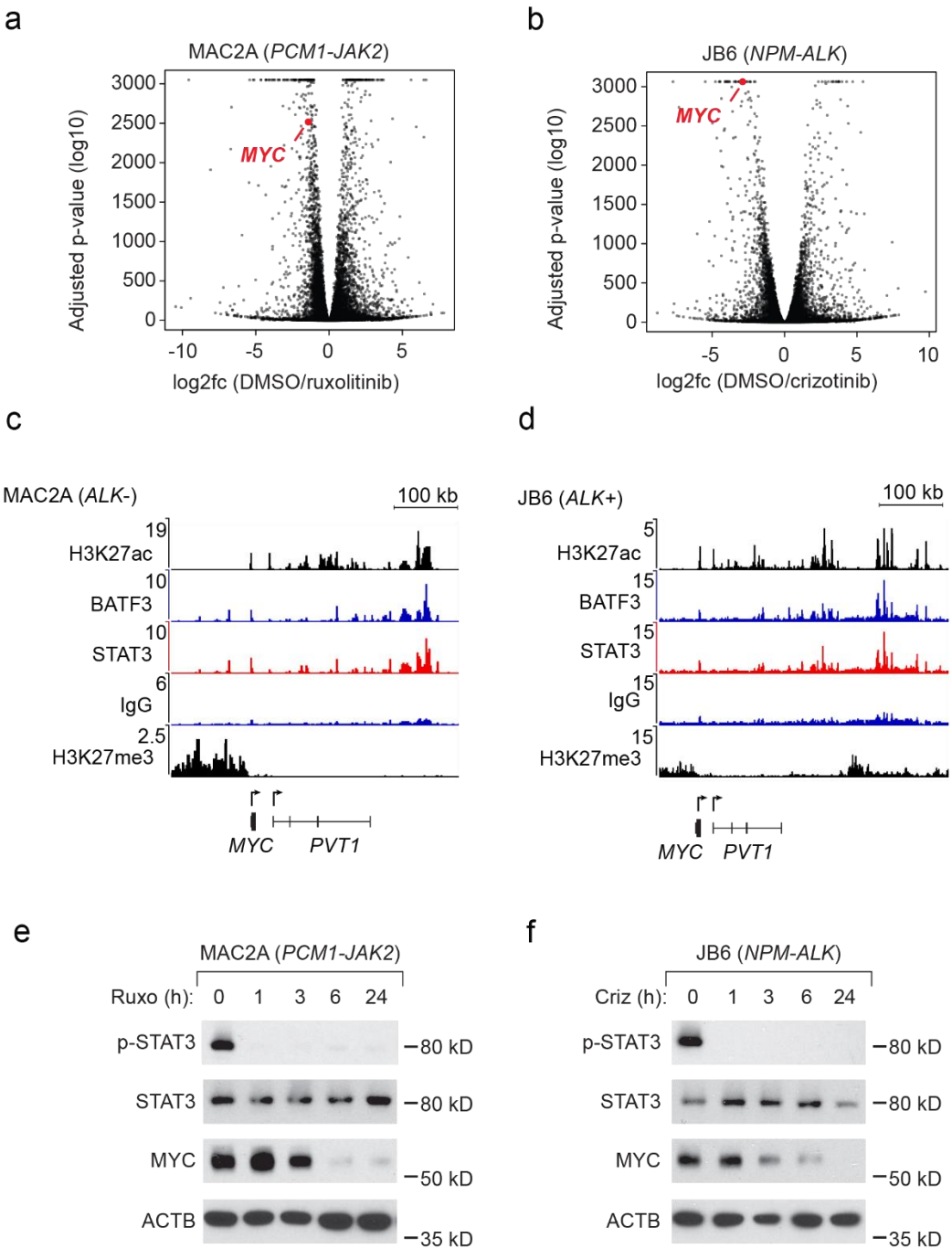

Figure 4. ALK or JAK inhibition attenuates STAT3-driven *MYC* expression. a-b) Volcano plot showing changes in transcript levels when MAC2A cells (a) were treated with ruxolitinib (JAK1- and JAK2-inhibitor) (1 μM, 24 hours) and when JB6 cells (b) were treated with crizotinib (ALK-inhibitor) (1 μM, 24 hours). c-d) ChIP-seq for H3K27ac and CUT&RUN sequencing alignment tracks for BATF3, STAT3 as well as IgG and H3K27me3 controls shown at the *MYC* gene locus in MAC2A (c) and JB6 (d) cells. e-f) Western blot time course showing the protein levels of phospho-STAT3 (Y705), total STAT3, MYC, and ACTB in MAC2A cells (e) treated with ruxolitinib (1 μM) and JB6 cells (f) treated with crizotinib (1 μM) for up to 24 hours.

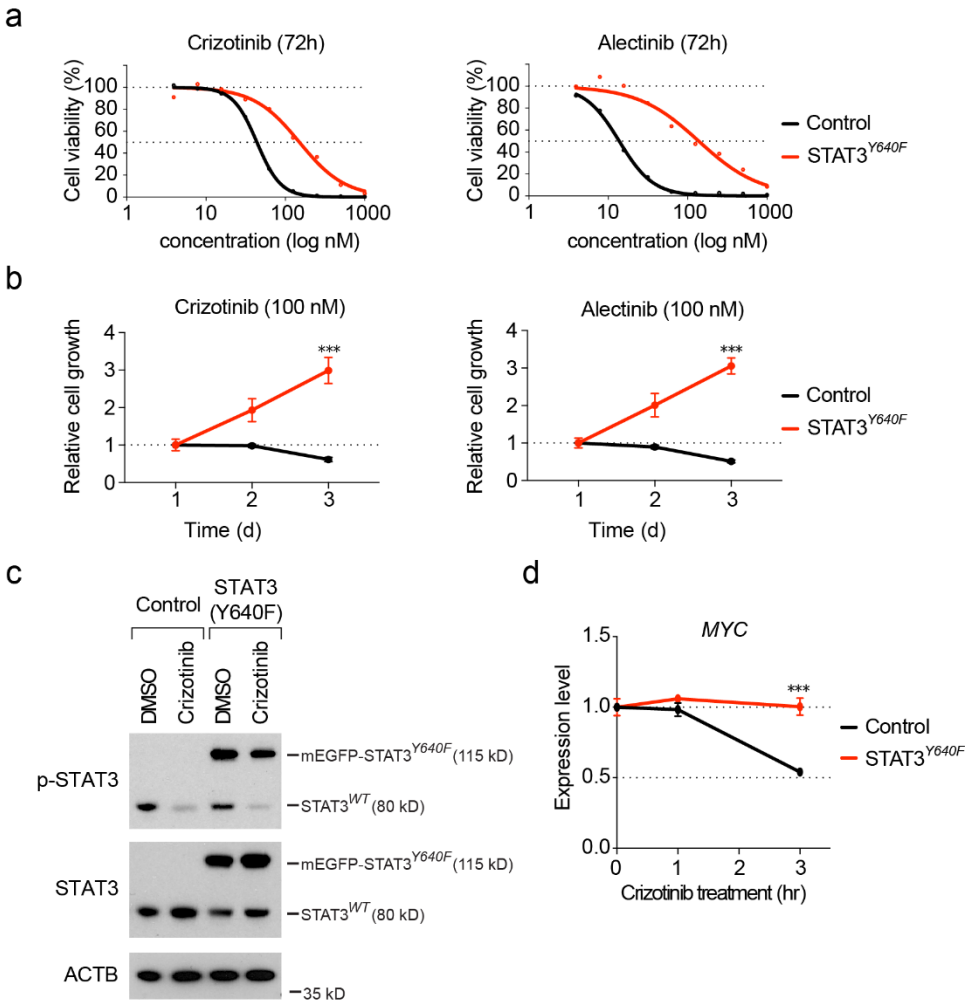

Figure 5. Expression of STAT3^{Y640F} rescues loss of cell growth and viability induced by ALK inhibition. a) Cell viability assays showing relative cell survival of control and STAT3^{Y640F} expressing JB6 cells treated with increasing concentrations of ALK inhibitors – crizotinib or alectinib – for 72 hours. b) Cell proliferation time course assay showing the relative growth of control and STAT3^{Y640F} JB6 cells treated with a single concentration of crizotinib or alectinib (100 nM) for up to 72 hours. c) Western blot for phospho-STAT3 (Y705), total STAT3 and β-actin in control, and STAT3^{Y640F} JB6 cells treated with DMSO, crizotinib (100 nM) for 6 hours. d) Quantitative PCR time course assaying *MYC* gene expression levels in JB6 control and STAT3^{Y640F} cells treated with crizotinib (100 nM) for 0, 1 and 3 hours, demonstrating that STAT3^{Y640F} expression rescued MYC expression at 3 hours ($p>0.001$).

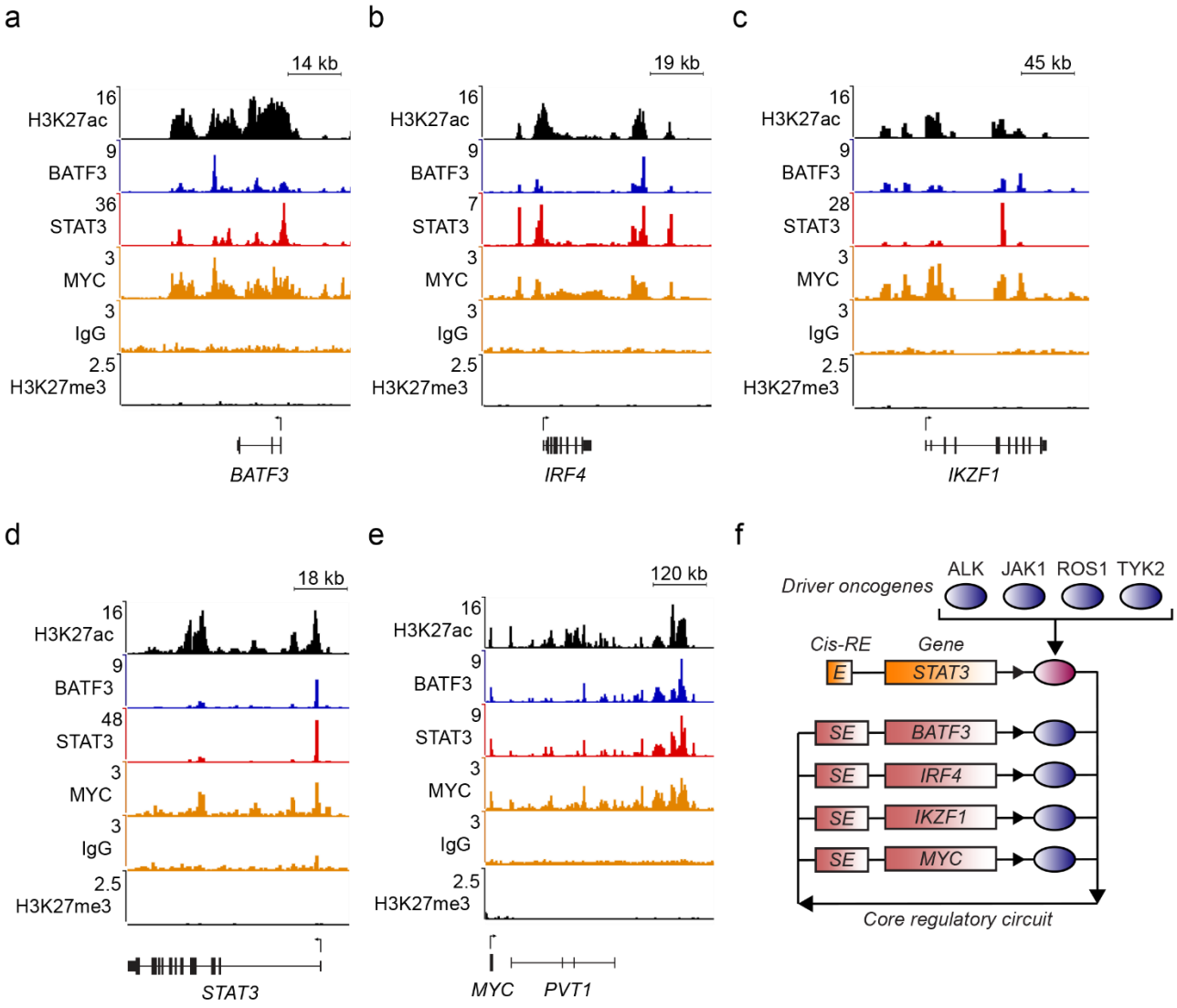

Figure 6. MYC invades super-enhancers driving CRC transcription factors. a-e) H3K27ac ChIP-seq and CUT&RUN sequencing alignment tracks for BATF3, STAT3, MYC as well as IgG and H3K27me3 controls in MAC2A cells, shown at the gene loci for *BATF3* (a), *IRF4* (b), *IKZF1* (c), STAT3 (d) and *MYC* (e). Read densities (y-axis) were normalized to reads per million reads sequenced in each sample. f) Illustration showing how BATF3, IRF4, IKZF1 and MYC form an interconnected co-regulatory loop together with STAT3, which is activated by dysregulation of ALK, JAK, ROS1, or TYK2. Rectangles illustrate regulatory elements, and gene loci and oval symbols illustrate proteins.

Resource availability

Lead Contact

Further information and requests for resources and reagents should be directed to and will be fulfilled by the Lead Contact, Mark W. Zimmerman (mwz2002@gmail.com).

Materials availability

All unique/stable reagents generated in this study are available from the Lead Contact with a completed Materials Transfer Agreement

Data and Code Availability

- Raw and processed data files were deposited to the NCBI GEO server under super-series GSE212077 and are publicly available as of the date of publication. Accession numbers are listed in the key resources table and in Supplemental data table S1.
- Software used for RNA-seq, ChIP-seq and CUT&RUN is publicly available from the indicated sources and the parameters used for analysis are listed in the detailed methods section of this paper.
- Any additional information required to reanalyze the data reported in this paper is available from the Lead Contact upon request.

Experimental model details

Patient-derived xenograft models

Both male and female NSG mice were purchased from the National Cancer Institute (Frederick, MD). Human ALCL patient-derived xenograft cells (line: WCTL-81162-Q13), obtained from the Dana-Farber Center for Patient-Derived Models, were subcutaneously implanted into the hind flanks of nine- to ten-week-old mice. When tumor volumes reached approximately 2000 mm^3, mice were euthanized, tumor cells were extracted and rinsed in PBS, fixed in PBS containing 1% formaldehyde for 10 min, washed with PBS, and snap-frozen in liquid nitrogen for ChIP-seq experiments. Experimental protocols were approved by the Dana–Farber Cancer Institute Animal Care and Use Committee (IACUC), and mice were maintained according to institutional guidelines.

Cell Lines

ALCL cell lines Karpas299, SUDHL1, JB6, SR-786, SUP-M2, FE-PD, MAC1, and MAC2A were obtained from ATCC. All cell lines were cultured in RPMI-1640 supplemented with 10% FBS and 100 IU/ml penicillin. Cells were tested for mycoplasma every 3 months with the Mycoalert kit (Promega), and identity was confirmed by STR profiling (DFCI molecular diagnostics laboratory). Cell proliferation assays were performed by seeding 5000 cells per well in 96-well plates containing DMSO, crizotinib, alectinib, iberidomide, Stattic, or STAT3-IN-3 (MedChemExpress, LLC). Cell viability was assayed with CellTiter-Glo according to the manufacturer's protocol (Promega).

Method details

Western blotting

Protein samples were collected and lysed using a radioimmunoprecipitation assay buffer containing protease and phosphatase inhibitors (Cell Signaling Technology). Lysates were quantified by Bradford assay (Bio-Rad), and 10 µg of extracted protein was separated using Novex SDS–polyacrylamide gel electrophoresis reagents and transferred to nitrocellulose membranes (Bio-Rad Laboratories). Membranes were blocked in 5% milk protein and incubated with primary antibodies overnight, followed by secondary horseradish peroxidase–linked goat anti-rabbit and anti-mouse antibodies (1:1000) according to the manufacturer's instructions. Antibody-bound membranes were incubated with SuperSignal West Pico chemiluminescent substrate (Thermo Fisher Scientific) and developed using HyBlot CL autoradiography film (Thomas Scientific). The antibodies used for immunoblotting are listed in Supplemental data table 1.

Quantitative RT-PCR

Total RNA was harvested using the RNeasy kit (QIAgen) according to the manufacturer's protocol. First-strand synthesis was performed with Superscript III (Invitrogen). Quantitative PCR analysis was conducted on the ViiA7 system (Life Technologies) with SYBR Green PCR Master Mix (Roche) using validated primers specific to each target each gene.

RNA-sequencing

RNA isolation was performed using the RNeasy Mini Kit (Qiagen), and RNA quality was assessed on a Fragment Analyzer (Advanced Analytical Technologies) − SS Total RNA 15nt. RNA-seq libraries were prepared using the Kapa mRNA HyperPrep Kit for Illumina (Roche) with Poly(A) selection according to the manufacturer's instructions. Library quantification was examined on a Fragment Analyzer − HS NGS Fragment 1-6000bp and Qubit HS dsDNA Kit (Invitrogen). Libraries were pooled and sequenced

to 150bp paired-end on the Illumina NovaSeq platform. Sequencing data were analyzed as described previously[59].

RNA-sequencing analysis

Raw reads were aligned to the hg19 revision of the human reference genome to which the sequences of the ERCC spike-in probes were added using hisat2[60] v2.1.0 in paired-end mode. Expression was quantified for all RefSeq genes downloaded 5/17/17 using htseq-count with parameters -i gene_id --stranded=reverse -m intersection-strict. Differential expression significance was determined statistically using DEseq2 and its Wald-derived test and read counts from each sample individually[60].

ChIP-sequencing and analysis

ChIP-seq was performed as previously described[50]. The antibodies used for each experiment are listed in Supplemental data table 1. For each ChIP, 5 µg of antibody coupled to 2 µg of magnetic Dynabeads (Life Technologies) was added to 3 ml of sonicated nuclear extract from formaldehyde-fixed cells. Chromatin was immunoprecipitated overnight, cross-links were reversed, and DNA was purified by precipitation with phenol:chloroform:isoamyl alcohol. DNA pellets were resuspended in 25 µl of TE buffer. Illumina sequencing, library construction, and ChIP-seq analysis methods were previously described. Reads were aligned to the human reference genome (hg19) using bowtie v1.2.2 with parameters –k 2 –m 2 –best and –l set to the read length. For visualization of single-end data, WIG files were created from aligned read positions using MACS v1.4 with parameters –w –S –space=50 –nomodel –shiftsize=200 to artificially extend reads to 200 bp and to calculate their density in 50-bp bins. For visualization of paired-end data, read-pairs were converted into fragments and used to quantify fragment coverage in 50bp genome-wide bins using bedtools makewindows and intersect. Read counts in 50-bp bins were normalized to the millions of mapped reads, giving RPM values. Converted bigWig files were visualized in the IGV browser version 2.16.2. The antibodies used for ChIP-seq are listed in the key resources table.

CUT&RUN sequencing and analysis

CUT&RUN sequencing was performed according to the manufacturer's protocol with slight adaptations (Epicypher). Concanavalin A (ConA) Conjugated Paramagnetic Beads (Fisher Scientific, #NC1526856) were initially activated using Bead Activation Buffer, containing 20 mM HEPES (pH 7.9), 10 mM KCl, 1 mM CaCl2, and 1 mM MnCl2. After activation, beads were washed and resuspended, preparing them for subsequent use. Cells were harvested and washed with RT Wash Buffer, and gently combined with the previously activated ConA beads to allow bead uptake by the cells. Next, antibodies for BATF3,

IRF4, IKZF1, STAT3, MYC, MED1, BRD4, H3K27me3 or IgG, were added to the cell-bead complexes for specific targeting and incubated overnight at 4 degrees Celsius on a rotator. The following day, the cell-bead complexes were subjected to several washing and resuspension steps using Digitonin Buffer (Wash Buffer containing 0.01% Digitonin). In the final phase, targeted chromatin digestion and release were achieved using 2.5 ul pAG-MNase (EpiCypher, #15-1016), alongside the addition of e. coli Spike-in DNA (1.0 ng) (EpiCypher, #18-1401). DNA purification was performed with the MinElute PCR purification kit (Qiagen, #28004). Illumina sequencing, library construction, and CUT&RUN-Seq analysis methods were previously described. Raw sequencing reads were aligned to the hg19 revision of the human reference genome using bowtie v1.2.2 in paired-end mode with parameters -k 2 -m 2 --best -X 600. For visualization of paired-end data, read alignments were converted into fragments using samtools view, samtools sort, and bedtools bamtobed. Fragment coverage was calculated in 50bp bins genome-wide using bedtools makewindows and bedtools intersect and were normalized to the millions of mapped reads. Converted bigWig files were visualized in the IGV browser version 2.16.2. The antibodies used for CUT&RUN sequencing are listed in the key resources table.

Patient-derived xenograft CUT&RUN-Seq processing

For patient-derived xenograft models, reads were first aligned to the mm9 revision of the mouse reference genome using bowtie v1.2.2 in paired-end mode with parameters -k 2 -m 2 –best and the non-mapping reads were retained using –un. For the remaining reads in the xenograft samples and all reads for other samples, reads were aligned to the human reference genome (hg19) using bowtie v1.2.2[61] with parameters –k 2 –m 2 –best and –l set to the read length. Paired-end samples were aligned in paired-end mode. For visualization of paired-end data, read-pairs were converted into fragments and used to quantify fragment coverage in 50bp genome-wide bins using bedtools makewindows and intersect. Read counts in 50-bp bins were normalized to the millions of mapped reads, giving RPM values. Converted bigWig files were visualized in the IGV browser version 2.7.2. The antibodies used for ChIP-seq are listed in Key Resources Table as stated above.

Super-enhancer identification and assignment

Super-enhancers in ALCL cells were identified in each cell line separately, as previously described[65] using ROSE (https://bitbucket.org/young_computation/rose). Reads overlapping ENCODE-defined problematic regions were removed from both H3K27ac and input BAM files using bedtools intersect against ENCFF001TDO. From the remaining reads, two sets of peaks of H3K27ac were identified using MACS, and the positions of aligned reads with parameter sets –keep-dup=auto –p 1e-9 and –keep-

dup=all –p 1e-9. The collapsed union of regions called using these MACS parameter sets was used as input for ROSE with parameters -s 12500 -t 1000 -g hg19. Enhancers were assigned to the single expressed gene, defined as being in the top two-thirds of the promoter (TSS ± 500 bp) H3K27ac coverage in a sample, whose transcription start site (TSS) was nearest the center of the enhancer.

Coverage heatmaps

Heatmaps showing coverage of purified sequence fragments (i.e., ChIP-Seq and CUT&RUN-Seq) were built at 4kb windows centered on the collapsed union of peaks for transcription factors. Peaks were identified using MACS v1.4 with corresponding control and reads and parameters -p 1e-9 –keep-dup=auto. Coverage of reads was quantified in these regions using bamToGFF (https://github.com/BradnerLab/pipeline/blob/master/bamToGFF.py) with parameter -m 50. Rows (regions) were ordered by the row sum of the H3K27ac signal.

CRISPR-Cas9 dependency screen analysis

Public data from genome-scale CRISPR-Cas9 screens performed at the Broad Institute were downloaded from FigShare (https://figshare.com/articles/dataset/DepMap_22Q2_Public/19700056/2). A total of n=1086 cancer cell lines (including n=5 ALCL lines) were screened with the Avana library, containing 73,372 guides and an average of 4 guides per gene[66]. The screens were conducted in a pooled experiment as previously described[29,67]. Genetic dependencies enriched in ALCL cell lines were identified using linear-model analysis from the limma v3.38.3 R package[68] by performing a two-tailed t-test for the difference in the distribution of gene dependency scores in ALCL compared to all other cell lines screened as previously described[28]. Statistical significance was calculated as a q-value derived from the p-value corrected for multiple hypothesis testing using the Benjamini & Hochberg method (https://www.jstor.org/stable/2346101). Transcription factor genes were highlighted based on a published list of human transcription factors[69].

Lentiviral transduction

The cDNA encoding mEGFP-tagged STAT3(Y640F), was synthesized and cloned into the pTwist lentiviral vector with puromycin resistance cassette at Twist Biosciences. ALCL cells were transduced with lentiviruses packaged and isolated from HEK293T cells. On Day 1, HEK293T cells were seeded and grown in DMEM medium to 60% confluency. On Day 2, pTwist-mEGFP-STAT3(Y640F) was co-transfected with psPAX2, and MD2.G packaging plasmids using Opti-MEM and FugeneHD according to the manufacturer's protocol (Promega). Media was replaced on Day 3 with complete RPMI medium

containing protamine sulfate. On Day 4, viral supernatant was collected, filtered, and stored. On Day 5, viral supernatant was collected again. For lentiviral transduction, experimental cells were resuspended in viral supernatant, centrifuged for 45 min at RT, and incubated with the virus for 48-72 hrs. Selection with puromycin was started at 72 hrs post-transduction, lasting 3 days.

Design and transfection of oligonucleotides

All nucleic acid (LNA) antisense oligonucleotides used in this study were 15-16 nucleotides in length and featured a phosphorothioate backbone. They contained a central DNA nucleotide flanked by LNA nucleotides at both the 5' and 3' ends. These ASOs were sourced from QIAGEN and designed using the QIAGEN Antisense GapmeR Designer. In each experiment, 1x10^6 cells were reverse-transfected with ASOs at a concentration of 1 μM (for BATF3, IRF4, IKZF1, MALAT1, and CTRL ASOs) or 10 μM (for MYCASO). Transfected cells were harvested for analysis within 24-72 hours and subjected to RNA extraction and qPCR.

Quantification and statistical analysis

Data from the ChIP-seq experiments were analyzed as described above. Cell viability data were analyzed with two-way ANOVA followed by post-hoc t-test. Statistical significance was defined as a p-value <0.05. Data were analyzed with GraphPad Prism 9.4.0, and all error bars represent SD unless otherwise noted.

Key resources table

REAGENT or RESOURCE	SOURCE	IDENTIFIER
Antibodies		
BATF3	R&D systems	Cat#AF7437
BRD4 (E2A7X)	Cell Signaling	Cat#13440
H3K27ac	Abcam	Cat#ab4729
IKZF1 (D6N9Y)	Cell Signaling	Cat#14859
IRF4 (D6P5H)	Cell Signaling	Cat#15106
MED1	Bethyl Laboratories	Cat#A300-793A
MYC	Cell Signaling	Cat#5605
STAT3 (D3Z2G)	Cell Signaling	Cat#126403
Mouse IgG	Santa Cruz Biotechnology	Cat#sc-2025
H3K27ac	Abcam	Cat#ab4729
H3K27me3	Abcam	Cat#ab192985
CUTANA Rabbit IgG	Epicypher	Cat#130042
p-STAT3 (Y705)	Cell Signaling	Cat#9145
STAT3 (124H6)	Cell Signaling	Cat#9139

BATF3	R&D systems	Cat#AF7437
IKZF1 (D6N9Y)	Cell Signaling	Cat#14859
IRF4 (D6P5H)	Cell Signaling	Cat#15106
p-STAT3 (Y705)	Cell Signaling	Cat#9145
STAT3	Cell Signaling	Cat#12640
ACTB	Cell Signaling	Cat#5970
Goat anti-Rabbit IgG (H+L) Secondary Antibody, HRP	Life Technologies	Cat#32460
Goat anti-Mouse IgG (H+L) Secondary Antibody, HRP	Thermo Fisher Scientific	Cat#62-6520
Bacterial and virus strains		
One shot Stbl 3 Chemically Competent *E. coli*	Invitrogen	Cat#C737303
Biological samples		
Patient-derived xenografts (PDX) ALCL sample	DFCI CPDM	WCTL-81162-Q13
Patient tumor (ALCL)	Liang et al.[55]	
Chemicals, peptides, and recombinant proteins		
Crizotinib	Medchem Express	Cat#HY-50878
Ruxolitinib	Medchem Express	Cat#HY-50856
Alectinib	Medchem Express	Cat#HY-13011
Thalidomide	Medchem Express	Cat#HY-14658
Lenalidomide	Medchem Express	Cat#HY-A0003
Avadomide	Medchem Express	Cat#HY-100507
Iberidomide	Medchem Express	Cat#HY-101291
STAT3-IN-3	Medchem Express	Cat#HY-128588
Stattic	Medchem Express	Cat#HY-13818
FuGene HD	Promega	Cat#E2311
Sodium chloride	Sigma Aldrich	Cat#S9888
Formaldehyde	Sigma Aldrich	Cat#252549
RNase	Thermo Fisher Scientific	Cat#EN0531
Triton X-100	Sigma Aldrich	Cat#T8787
DMSO	Fisher Scientific	Cat#BP231-100
HEPES	Life Technologies	Cat#15630080
CaCl2	Thermo Fisher Scientific	Cat#AAJ63122AE
MnCl2	Sigma Aldrich	Cat#M1028
Spermidine trihydrochloride	Sigma Aldrich	Cat#S2501
Digitonin	Sigma Aldrich	Cat#300410
EDTA	Thermo Fisher Scientific	Cat#AM9260G
EGTA	Westnet. Inc.	Cat#BM-151
KCL	Invitrogen	Cat#AM9640G
Glycogen	Thermo Fisher Scientific	Cat# R0561
Critical commercial assays		
Concanavalin A (ConA) Conjugated Paramagnetic Beads	Fisher Scientific	Cat#NC1526856
MinElute PCR purification kit	Qiagen	Cat#28004

Dynabeads Antibody Coupling Kit	Invitrogen	Cat#14311D
pAG-MNase	EpiCypher	Cat#15-1016
E. coli Spike-in DNA	EpiCypher	Cat#18-1401
ERCC RNA Spike-In Mix	Thermo Fisher Scientific	Cat#4456740
FastStart Universal SYBR Green Master (Rox)	Millipore SIGMA	Cat#4913914001
RNeasy MINI kit	Qiagen	Cat#74104
SuperScript™ III	Thermo Fisher Scientific	Cat#12574026
CellTiter-Glo	Promega	Cat#G7570
Deposited data		
Raw and analyzed ChIP-seq, CUT&RUN and RNA-seq data (for details see samples listed below and in Table S1)	This paper	GEO: GSE212077
ChIP-seq samples:		
K299, H3K27ac	Liang et al.[55]	GSM4815740
K299, Input	Liang et al.[55]	GSM4815739
JB6, H3K27ac	Liang et al.[55]	GSM5277976
JB6, Input	Liang et al.[55]	GSM5277975
SR786, H3K27ac	Liang et al.[55]	GSM5277980
SR786, Input	Liang et al.[55]	GSM5277979
SUDHL1, H3K27ac	Liang et al.[55]	GSM5277982
SUDHL1, Input	Liang et al.[55]	GSM5277981
SUPM2, H3K27ac	This paper	GSM6508942
SUPM2, Input	This paper	GSM6508943
MAC1, H3K27ac	Liang et al.[55]	GSM4815743
MAC1, Input	Liang et al.[55]	GSM4815742
MAC2A, H3K27ac	Liang et al.[55]	GSM5277986
MAC2A, Input	Liang et al.[55]	GSM5277985
FE-PD, H3K27ac	Liang et al.[55]	GSM5277984
FE-PD, Input	Liang et al.[55]	GSM5277983
Patient tumor (ALCL), H3K27ac	Liang et al.[55]	GSM5277988
Patient tumor (ALCL), Input	Liang et al.[55]	GSM5277987
PDX (ALK+ ALCL), H3K27ac	This paper	GSM6508944
PDX (ALK+ ALCL), BATF3	This paper	GSM6508945
PDX (ALK+ ALCL), STAT3	This paper	GSM6508946
PDX (ALK+ ALCL), Input	This paper	GSM6508947
Cut & Run samples:		
MAC2A, MED1 (Ctrl = IgG_1)	This paper	GSM6508924
MAC2A, BRD4 (Ctrl = IgG 2)	This paper	GSM6508925
MAC2A, BATF3 (Ctrl = IgG_1)	This paper	GSM6508926
MAC2A, IRF4 (Ctrl = IgG_1)	This paper	GSM6508927
MAC2A, IKZF1(Ctrl = IgG_1)	This paper	GSM6508928
MAC2A, STAT3 (Ctrl = IgG 2)	This paper	GSM6508929
MAC2A, MYC (Ctrl = IgG 3)	This paper	GSM6508930
MAC2A, H3K27me3 (Ctrl = IgG 4)	This paper	GSM8059295

MAC2A, IgG_1	This paper	GSM8059298
MAC2A, IgG_2	This paper	GSM6508931
MAC2A, IgG_3	This paper	GSM8059296
MAC2A, IgG_4	This paper	GSM8059297
JB6, BATF3 (Ctrl = IgG_1)	This paper	GSM6508932
JB6, STAT3 (Ctrl = IgG_1)	This paper	GSM6508933
JB6, MYC (Ctrl = IgG_2)	This paper	GSM6508935
JB6, H3K27me3 (Ctrl = IgG_3)	This paper	GSM8059292
JB6, IgG_1	This paper	GSM6508934
JB6, IgG_2	This paper	GSM8059293
JB6, IgG_3	This paper	GSM8059294
RNA-seq samples:		
JB6 (replicate 1), DMSO	This paper	GSM6508865
JB6 (replicate 2), DMSO	This paper	GSM6508866
JB6 (replicate 3), DMSO	This paper	GSM6508867
JB6 (replicate 1), Crizotinib (1mM, 24h)	This paper	GSM6508868
JB6 (replicate 2), Crizotinib (1mM, 24h)	This paper	GSM6508869
JB6 (replicate 3), Crizotinib (1mM, 24h)	This paper	GSM6508870
MAC2A (replicate 1), DMSO	This paper	GSM6508871
MAC2A (replicate 2), DMSO	This paper	GSM6508872
MAC2A (replicate 3), DMSO	This paper	GSM6508873
MAC2A (replicate 1), Ruxolitinib (1mM, 24h)	This paper	GSM6508874
MAC2A (replicate 2), Ruxolitinib (1mM, 24h)	This paper	GSM6508875
MAC2A (replicate 3), Ruxolitinib (1mM, 24h)	This paper	GSM6508876
Experimental models: Cell lines		
Karpas299 (K299)	Prof. Merkel, Medical University of Vienna, Austria	RRID:CVCL_V404
JB6	Prof. Merkel, Medical University of Vienna, Austria	RRID:CVCL_H633
SR786	DSMZ	ACC 369
SUDHL1	ATCC	CRL-2955
SUPM2	DSMZ	Cat#ACC 509
MAC1	Prof. Merkel, Medical University of Vienna, Austria	RRID:CVCL_H631
MAC2A	Prof. Merkel, Medical University of Vienna, Austria	RRID:CVCL_H637
FE-PD	Prof. Merkel, Medical University of Vienna, Austria	RRID:CVCL_H614
HEK293T	ATCC	Cat#CRL-3216, RRID:CVCL_0063
Experimental models: Organisms/strains		
NOD.Cg-Prkdcscid Il2rgtm1Wjl/SzJ	The Jackson Laboratory	RRID:IMSR_JAX:005557

Oligonucleotides		
ACTB fw: AGAGCTACGAGCTGCCTGAC	This paper	N/A
ACTB rev: AGCACTGTGTTGGCGTACAG	This paper	N/A
BATF3 fw: GTTGCTGCTCAGAGAAGTCGG	This paper	N/A
BATF3 rev: TCTCCGCAGCATGGTGTTTTC	This paper	N/A
IRF4 fw: AGCCACTACGTCCCGGATCA	This paper	N/A
IRF4 rev: CGGCAGACCTTATGCTTGGC	This paper	N/A
IKZF1 fw: CTGGCAGGGCAGAGGGAG	This paper	N/A
IKZF1 rev: GGGGGCTTTCCTTCCCTGAA	This paper	N/A
MYC fw: GCTGCTTAGACGCTGGATTT	Gill et al.[64]	N/A
MYC rev: CTCCTCCTCGTCGCAGTAGA	Gill et al.[64]	N/A
MYCASO-3: 5'-TTCACCATGTCTCCTC-3'	Gill et al.[64]	N/A
MYCASO-9: 5'-GGTACAAGCTGGAGGT-3'	Gill et al.[64]	N/A
MYCASO-13: 5'-GTAGTTGTGCTGATGT-3'	Gill et al.[64]	N/A
BATF3 ASO: 5'-GGGACAGCGCCCGT-3'	Qiagen	N/A
IKZF1 ASO: 5'-GGGCCCGGCGCGG-3'	Qiagen	N/A
IRF4 ASO: 5'-ACCTCGCACTCTCAG-3'	Qiagen	N/A
MALAT1 ASO	Qiagen	N/A
Negative Control ASO	Qiagen	N/A
Recombinant DNA		
Plasmid: pTwist-mEGFP-STAT3(Y640F) Puro	Twist biosciences	N/A
Plasmid: psPAX	Addgene	Cat#12259
Plasmid: pMD2.G	Addgene	Cat#12260
Software and algorithms		
GraphPad Prism (Version 9.4.0)	GraphPad	RRID:SCR_002798
Microsoft Excel	Microsoft	RRID:SCR_016137
IGV (Version 2.16.2)	Thorvaldsdóttir et al.[65]	RRID:SCR_011793
ROSE	Whyte et al.[19] and Loven et al.[66]	RRID:SCR_017390
MACS v1.4	Zhang et al.[67]	RRID:SCR_013291
SAMTOOLS	Li et al.[68]	RRID:SCR_002105
BEDTools	Quinlan et al.[69]	RRID:SCR_006646
Makewindows	Quinlan et al.[69]	
Intersect	Quinlan et al.[69]	
bamToGFF	Loven et al.[66]	
Other		
Novex 4-20% Tris-Glycine Mini Gels, WedgeWell format, 12-well	Life Technologies	Cat#XP04202BOX
Bradford Reagent	Bio-Rad Laboratories	Cat#500-0205
Nitrocellulose Membrane	Bio-Rad Laboratories	Cat#1620112
labForce HyBlot CL® Autoradiography Film, 5 x 7"	Thomas Scientific	Cat#1141J51
cOmplete Mini EDTA-free Protease Inhibitor Cocktail	Sigma-Aldrich	Cat#11836170001
Super Signal West Pico PLUS Chemiluminescent Substrate	Thermo Fisher Scientific	Cat#34580
RPMI 1640 Medium	Thermo Fisher Scientific	Cat#11875093

FBS	Thermo Fisher Scientific	Cat#16000044
PBS	Thermo Fisher Scientific	Cat#10010023
DMEM Dulbecco's Modified Eagle Medium	Thermo Fisher Scientific	Cat#11995073
TE Buffer	Life Technologies	Cat#AM9849

References

1. Morris, S. W. *et al.* Fusion of a kinase gene, ALK, to a nucleolar protein gene, NPM, in non-Hodgkin's lymphoma. *Science* **263**, 1281–1284 (1994).
2. Le Beau, M. M. *et al.* The t(2;5)(p23;q35): a recurring chromosomal abnormality in Ki-1-positive anaplastic large cell lymphoma. *Leukemia* **3**, 866–870 (1989).
3. Kaneko, Y. *et al.* A novel translocation, t(2;5)(p23;q35), in childhood phagocytic large T-cell lymphoma mimicking malignant histiocytosis. *Blood* **73**, 806–813 (1989).
4. Rimokh, R. *et al.* A translocation involving a specific breakpoint (q35) on chromosome 5 is characteristic of anaplastic large cell lymphoma ('Ki-1 lymphoma'). *Br J Haematol* **71**, 31–36 (1989).
5. Leventaki, V., Bhattacharyya, S. & Lim, M. S. Pathology and genetics of anaplastic large cell lymphoma. *Semin Diagn Pathol* **37**, 57–71 (2020).
6. Stein, H. *et al.* The expression of the Hodgkin's disease associated antigen Ki-1 in reactive and neoplastic lymphoid tissue: evidence that Reed-Sternberg cells and histiocytic malignancies are derived from activated lymphoid cells. *Blood* **66**, 848–858 (1985).
7. Laimer, D. *et al.* PDGFR blockade is a rational and effective therapy for NPM-ALK-driven lymphomas. *Nat Med* **18**, 1699–1704 (2012).
8. Iqbal, J. *et al.* Genomic signatures in T-cell lymphoma: How can these improve precision in diagnosis and inform prognosis? *Blood Rev* **30**, 89–100 (2016).
9. Cairo, M. S. & Beishuizen, A. Childhood, adolescent and young adult non-Hodgkin lymphoma: current perspectives. *Br J Haematol* **185**, 1021–1042 (2019).
10. Prokoph, N., Larose, H., Lim, M. S., Burke, G. A. A. & Turner, S. D. Treatment Options for Paediatric Anaplastic Large Cell Lymphoma (ALCL): Current Standard and beyond. *Cancers (Basel)* **10**, E99 (2018).
11. Gambacorti-Passerini, C. *et al.* Long-term effects of crizotinib in ALK-positive tumors (excluding NSCLC): A phase 1b open-label study. *Am J Hematol* **93**, 607–614 (2018).
12. Crescenzo, R. *et al.* Convergent mutations and kinase fusions lead to oncogenic STAT3 activation in anaplastic large cell lymphoma. *Cancer Cell* **27**, 516–532 (2015).
13. Prutsch, N. *et al.* Dependency on the TYK2/STAT1/MCL1 axis in anaplastic large cell lymphoma. *Leukemia* **33**, 696–709 (2019).
14. Chen, J. *et al.* Cytokine receptor signaling is required for the survival of ALK- anaplastic large cell lymphoma, even in the presence of JAK1/STAT3 mutations. *Proc Natl Acad Sci U S A* **114**, 3975–3980 (2017).

15. Hapgood, G. & Savage, K. J. The biology and management of systemic anaplastic large cell lymphoma. *Blood* **126**, 17–25 (2015).
16. Stark, G. R. & Darnell, J. E. The JAK-STAT pathway at twenty. *Immunity* **36**, 503–514 (2012).
17. Levy, D. E. & Darnell, J. E. Stats: transcriptional control and biological impact. *Nat Rev Mol Cell Biol* **3**, 651–662 (2002).
18. Saint-André, V. *et al.* Models of human core transcriptional regulatory circuitries. *Genome Res.* **26**, 385–396 (2016).
19. Whyte, W. A. *et al.* Master transcription factors and mediator establish super-enhancers at key cell identity genes. *Cell* **153**, 307–319 (2013).
20. Parker, S. C. J. *et al.* Chromatin stretch enhancer states drive cell-specific gene regulation and harbor human disease risk variants. *Proc Natl Acad Sci U S A* **110**, 17921–17926 (2013).
21. Zamo, A. *et al.* Anaplastic lymphoma kinase (ALK) activates Stat3 and protects hematopoietic cells from cell death. *Oncogene* **21**, 1038–1047 (2002).
22. Sanda, T. *et al.* Core transcriptional regulatory circuit controlled by the TAL1 complex in human T cell acute lymphoblastic leukemia. *Cancer Cell* **22**, 209–221 (2012).
23. Durbin, A. D. *et al.* Selective gene dependencies in MYCN-amplified neuroblastoma include the core transcriptional regulatory circuitry. *Nat. Genet.* **50**, 1240–1246 (2018).
24. Hnisz, D. *et al.* Convergence of developmental and oncogenic signaling pathways at transcriptional super-enhancers. *Mol Cell* **58**, 362–370 (2015).
25. Ghandi, M. *et al.* Next-generation characterization of the Cancer Cell Line Encyclopedia. *Nature* **569**, 503–508 (2019).
26. Jahangiri, L. *et al.* Core regulatory circuitries in defining cancer cell identity across the malignant spectrum. *Open Biol* **10**, 200121 (2020).
27. Ng, S. Y. *et al.* Targetable vulnerabilities in T- and NK-cell lymphomas identified through preclinical models. *Nat Commun* **9**, 2024 (2018).
28. Dharia, N. V. *et al.* A first-generation pediatric cancer dependency map. *Nat Genet* **53**, 529–538 (2021).
29. Meyers, R. M. *et al.* Computational correction of copy number effect improves specificity of CRISPR-Cas9 essentiality screens in cancer cells. *Nat Genet* **49**, 1779–1784 (2017).
30. Bai, L. *et al.* A Potent and Selective Small-Molecule Degrader of STAT3 Achieves Complete Tumor Regression In Vivo. *Cancer Cell* **36**, 498-511.e17 (2019).
31. Yamamoto, T. *et al.* The nuclear isoform of protein-tyrosine phosphatase TC-PTP regulates interleukin-6-mediated signaling pathway through STAT3 dephosphorylation. *Biochem Biophys Res Commun* **297**, 811–817 (2002).

32. Shields, B. J. *et al.* TCPTP regulates SFK and STAT3 signaling and is lost in triple-negative breast cancers. *Mol Cell Biol* **33**, 557–570 (2013).
33. Kleppe, M. *et al.* PTPN2 negatively regulates oncogenic JAK1 in T-cell acute lymphoblastic leukemia. *Blood* **117**, 7090–7098 (2011).
34. Karaca Atabay, E. *et al.* Tyrosine phosphatases regulate resistance to ALK inhibitors in ALK+ anaplastic large cell lymphoma. *Blood* **139**, 717–731 (2022).
35. El Kasmi, K. C. *et al.* Cutting edge: A transcriptional repressor and corepressor induced by the STAT3-regulated anti-inflammatory signaling pathway. *J Immunol* **179**, 7215–7219 (2007).
36. Prokoph, N. *et al.* IL10RA modulates crizotinib sensitivity in NPM1-ALK+ anaplastic large cell lymphoma. *Blood* **136**, 1657–1669 (2020).
37. Darnell, J. E., Kerr, I. M. & Stark, G. R. Jak-STAT pathways and transcriptional activation in response to IFNs and other extracellular signaling proteins. *Science* **264**, 1415–1421 (1994).
38. Chiarle, R. *et al.* Stat3 is required for ALK-mediated lymphomagenesis and provides a possible therapeutic target. *Nat Med* **11**, 623–629 (2005).
39. Zhang, Q. *et al.* Multilevel dysregulation of STAT3 activation in anaplastic lymphoma kinase-positive T/null-cell lymphoma. *J Immunol* **168**, 466–474 (2002).
40. Nie, Z. *et al.* c-Myc is a universal amplifier of expressed genes in lymphocytes and embryonic stem cells. *Cell* **151**, 68–79 (2012).
41. Lin, C. Y. *et al.* Transcriptional amplification in tumor cells with elevated c-Myc. *Cell* **151**, 56–67 (2012).
42. Zeid, R. *et al.* Enhancer invasion shapes MYCN-dependent transcriptional amplification in neuroblastoma. *Nat. Genet.* **50**, 515–523 (2018).
43. See, Y. X., Chen, K. & Fullwood, M. J. MYC overexpression leads to increased chromatin interactions at super-enhancers and MYC binding sites. *Genome Res* **32**, 629–642 (2022).
44. Harrison, D. A. The Jak/STAT pathway. *Cold Spring Harb Perspect Biol* **4**, a011205 (2012).
45. Sever, R. & Brugge, J. S. Signal transduction in cancer. *Cold Spring Harb Perspect Med* **5**, a006098 (2015).
46. Brooks, A. J. & Putoczki, T. JAK-STAT Signalling Pathway in Cancer. *Cancers (Basel)* **12**, E1971 (2020).
47. Ohgami, R. S. *et al.* STAT3 mutations are frequent in CD30+ T-cell lymphomas and T-cell large granular lymphocytic leukemia. *Leukemia* **27**, 2244–2247 (2013).
48. Chiarle, R., Voena, C., Ambrogio, C., Piva, R. & Inghirami, G. The anaplastic lymphoma kinase in the pathogenesis of cancer. *Nat Rev Cancer* **8**, 11–23 (2008).

49. Chapuy, B. *et al.* Discovery and characterization of super-enhancer-associated dependencies in diffuse large B cell lymphoma. *Cancer Cell* **24**, 777–790 (2013).
50. Wong, R. W. J. *et al.* Enhancer profiling identifies critical cancer genes and characterizes cell identity in adult T-cell leukemia. *Blood* **130**, 2326–2338 (2017).
51. Mack, S. C. *et al.* Therapeutic targeting of ependymoma as informed by oncogenic enhancer profiling. *Nature* **553**, 101–105 (2018).
52. Liu, Q., Guo, L., Lou, Z., Xiang, X. & Shao, J. Super-enhancers and novel therapeutic targets in colorectal cancer. *Cell Death Dis* **13**, 228 (2022).
53. Liang, H.-C. *et al.* Super-enhancer-based identification of a BATF3/IL-2R-module reveals vulnerabilities in anaplastic large cell lymphoma. *Nat Commun* **12**, 5577 (2021).
54. Bandini, C. *et al.* IRF4 Mediates the Oncogenic Effects of STAT3 in Anaplastic Large Cell Lymphomas. *Cancers (Basel)* **10**, E21 (2018).
55. Liang, H.-C. *et al.* Super-enhancer-based identification of a BATF3/IL-2R-module reveals vulnerabilities in anaplastic large cell lymphoma. *Nat Commun* **12**, 5577 (2021).
56. Schleussner, N. *et al.* The AP-1-BATF and -BATF3 module is essential for growth, survival and TH17/ILC3 skewing of anaplastic large cell lymphoma. *Leukemia* **32**, 1994–2007 (2018).
57. Gryder, B. E. *et al.* Histone hyperacetylation disrupts core gene regulatory architecture in rhabdomyosarcoma. *Nat Genet* **51**, 1714–1722 (2019).
58. Zamudio, A. V. *et al.* Mediator Condensates Localize Signaling Factors to Key Cell Identity Genes. *Mol Cell* **76**, 753-766.e6 (2019).
59. Mullen, A. C. *et al.* Master transcription factors determine cell-type-specific responses to TGF-β signaling. *Cell* **147**, 565–576 (2011).
60. Alitalo, K., Schwab, M., Lin, C. C., Varmus, H. E. & Bishop, J. M. Homogeneously staining chromosomal regions contain amplified copies of an abundantly expressed cellular oncogene (c-myc) in malignant neuroendocrine cells from a human colon carcinoma. *Proc Natl Acad Sci U S A* **80**, 1707–1711 (1983).
61. Nowell, P. *et al.* Association of amplified oncogene c-myc with an abnormally banded chromosome 8 in a human leukaemia cell line. *Nature* **306**, 494–497 (1983).
62. Affer, M. *et al.* Promiscuous MYC locus rearrangements hijack enhancers but mostly super-enhancers to dysregulate MYC expression in multiple myeloma. *Leukemia* **28**, 1725–1735 (2014).
63. Zimmerman, M. W. *et al.* MYC Drives a Subset of High-Risk Pediatric Neuroblastomas and Is Activated through Mechanisms Including Enhancer Hijacking and Focal Enhancer Amplification. *Cancer Discov* **8**, 320–335 (2018).

64. Gill, T. *et al.* Selective targeting of MYC mRNA by stabilized antisense oligonucleotides. *Oncogene* **40**, 6527–6539 (2021).
65. Thorvaldsdóttir, H., Robinson, J. T. & Mesirov, J. P. Integrative Genomics Viewer (IGV): high-performance genomics data visualization and exploration. *Brief Bioinform* **14**, 178–192 (2013).
66. Lovén, J. *et al.* Selective inhibition of tumor oncogenes by disruption of super-enhancers. *Cell* **153**, 320–334 (2013).
67. Zhang, Y. *et al.* Model-based analysis of ChIP-Seq (MACS). *Genome Biol* **9**, R137 (2008).
68. Li, H. & Durbin, R. Fast and accurate short read alignment with Burrows-Wheeler transform. *Bioinformatics* **25**, 1754–1760 (2009).
69. Quinlan, A. R. & Hall, I. M. BEDTools: a flexible suite of utilities for comparing genomic features. *Bioinformatics* **26**, 841–842 (2010).